

Multifunctional design of prismatic cellular materials

CAROLYN C. SEEPERSAD, RAJESH S. KUMAR, JANET K. ALLEN,
FARROKH MISTREE and DAVID L. MCDOWELL*

*G.W. Woodruff School of Mechanical Engineering, Georgia Institute of Technology, Atlanta,
GA 30332-0405, USA*

Received 12 April 2004; Accepted 15 September 2004

Abstract. Low density, prismatic cellular materials have a combination of properties that make them suitable for multifunctional or multi-physics applications such as ultralight load-bearing combined with energy absorption and heat transfer. In this work, non-uniform, graded cellular materials are designed to achieve superior thermal and structural performance. A general multifunctional design approach is presented that integrates multiobjective decision-making with multi-physics analysis tools of structural and heat transfer performance. Approximate analysis models for heat transfer and elastic stiffness are utilized to analyze designs efficiently. Search/solution algorithms are used to solve multi-objective decisions by interfacing with customized and commercial software. During the design process, cell topology is assumed to be rectangular, but aspect ratios and dimensions of cells and cell walls are varied. Two design scenarios are considered – maximum convective heat transfer and in-plane elastic stiffness in the first case and maximum convective heat transfer and elastic buckling strength in the second case. A portfolio of heat exchanger designs is generated with both periodic and functionally graded cells. Both single- and multi-objective performance are considered, and trade-offs are assessed between thermal and structural performance. Generalization of this approach is discussed for broader materials design applications in which material structures and processing paths are designed to achieve targeted properties and performance characteristics within a larger overall systems design process, and process-structure-property-performance relations are manifested on a hierarchy of length and time scales.

Keywords: compromise decision support problem, convective heat transfer, elastic buckling, elastic stiffness, finite difference, finite element, honeycombs, linear cellular alloys, multifunctional design, multiobjective decisions

1. Frame of reference: Designing multifunctional, prismatic cellular materials

Materials design has traditionally involved selecting a suitable material for a given application. Presently, a paradigm shift is underway in which the classical materials selection approach is replaced by design of material microstructure or mesostructure to achieve certain performance requirements, subject to constraints on properties such as density, strength, conductivity, etc. Mechanics models play a central role in evaluating and predicting the performance metrics necessary to support design of heterogeneous materials. By utilizing these models along with systems-based design methods, material microstructure or mesostructure can be tailored or designed for specific performance requirements associated with applications of interest.

*To whom correspondence should be addressed. E-mail: david.mcdowell@me.gatech.edu

Prismatic cellular materials, essentially extruded metal honeycombs, are well-suited for multifunctional applications in which the material is required to meet multiple performance objectives. Prismatic cellular materials have a combination of properties that can be tailored to make them suitable for a range of applications such as ultra-light structures, heat exchangers, fuel cell and battery subsystems, energy absorption systems, and others [1–3]. Newly developed, flexible manufacturing processes enable extensive tailoring of prismatic cellular materials for multifunctional applications. For example, via a thermo-chemical extrusion fabrication process developed at Georgia Tech, based on hydrogen reduction of extruded metal oxide powder slurries, prismatic cellular materials (so-called Linear Cellular Alloys (LCAs)) can be produced with nearly arbitrary two-dimensional topologies, metallic base materials, and wall thicknesses as small as $50\ \mu\text{m}$ [4].

Several authors have reported multifunctional analyses of prismatic cellular materials (c.f., [1–3, 5]). However, these authors focus on determining the thermal and structural properties of a set of standard cellular topologies such as periodic hexagonal, triangular, and square cells. The authors emphasize *selection* among a standard set of cellular designs, which restricts choices to cellular topologies that are currently available and well characterized. By tailoring, adjusting, or *designing* the cellular topology, geometry, and dimensions (i.e., the cellular material mesostructure), it may be possible to achieve preferred or improved multifunctional performance via novel cell types, functionally graded cellular arrangements, and dimensional adjustments.

In this paper, we focus on *designing* prismatic cellular materials for multifunctional applications. The internal mesostructure of these materials is designed by systematically adjusting the number, geometric aspect ratios, and dimensions of cells and cell walls throughout a cellular material. The objective is to achieve superior multifunctional performance, subject to fabrication- and physics-based constraints. Our design approach is multifunctional – founded in multiobjective decision support and systems-based approaches. Our approach requires relatively fast, accurate techniques for analyzing performance in thermal and mechanical domains, as outlined in Section 3. The multifunctional analysis techniques are utilized as part of a multifunctional design approach anchored in multiobjective decision-making, as described in Section 4. To demonstrate our approach, we design structural heat exchangers for an application that demands superior thermal and structural properties, as outlined in the following section. Whereas our approach is demonstrated for the design of cellular mesostructure, it is extensible as a systems-based design approach for more complex materials design problems in which process-structure-property-performance relations are manifested on a hierarchy of length and time scales, as discussed in Section 6.

2. Designing a structural heat exchanger comprised of prismatic cellular material

Prismatic cellular materials are potentially well-suited for heat exchanger applications, including compact electronic cooling devices and ultra-light, actively cooled, aerospace structures. Unlike most heat exchangers, however, the two-dimensional cells that dissipate heat via conduction and convection may be required to serve a structural function, for example actively cooled skins in high performance aerospace vehicles. Our goal for the present example is to determine appropriate cell aspect ratios and sizes to achieve desirable values for objectives from two distinct physical

domains: (1) overall rate of steady state heat transfer and (2) overall structural elastic stiffness and critical elastic buckling load of the material.

The device illustrated in Figure 1 is a sample compact heat exchanger for a representative electronic cooling application in which the device is required to dissipate heat and support structural loads. The device has fixed overall width (W), depth (D), and height (H) of 25 mm, 75 mm, and 25 mm, respectively. It is insulated on the left, right, and bottom sides and is subjected to a heat source at constant temperature, T_s , on the top face. The mechanism for heat dissipation is forced convection via air with entry temperature, T_{in} , and total mass flow rate \dot{M} . The flow rate is variable, but it is linked to the available pressure head through a characteristic fan curve. As illustrated in Figure 2, the operational flow rate is determined by the intersection of the solid fan curve with the dotted LCA system curve that is dependent on cellular configuration and dimensions. Steady state, incompressible laminar flow is assumed. The solid material in the device is copper. The thermal conductivity, k_s , of copper samples fabricated with the thermo-chemical extrusion process has been measured to be 363 W/m-K [6]. For evaluation of the critical elastic buckling load of a prismatic cellular material, a uniformly distributed load is applied on the top surface in addition

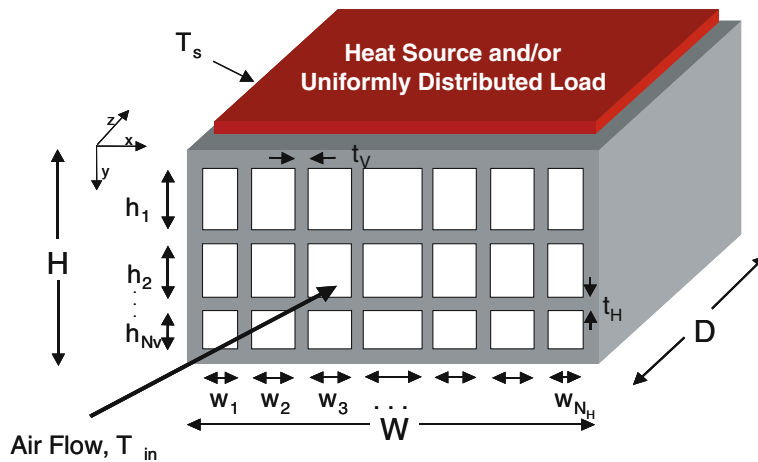


Figure 1. Compact, forced convection heat exchanger with graded, rectangular, prismatic, cellular materials.

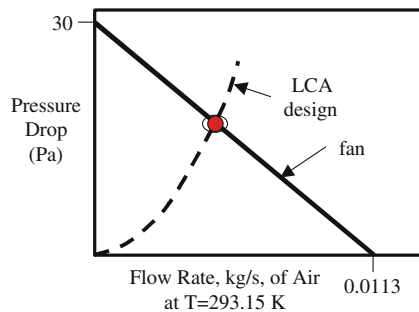


Figure 2. Characteristic fan curve.

to the heat source. The bottom and remaining surfaces are considered as fixed and free boundaries, respectively.

For this example, the prismatic cellular material is comprised exclusively of rectangular cells, but the size, shape (i.e., aspect ratio), and number of cells are permitted to vary in a graded manner. In a graded material, each row of cells may assume a different height, h_i , and each column a different width, w_i . The only restriction on cell height and width is that the cells must fit within the external dimensions with sufficient remaining space for vertical cell walls of variable thickness, t_v , and horizontal walls of variable thickness, t_h . The numbers of cells in the horizontal and vertical directions are designated N_H and N_V , respectively.

3. Structural and thermal analysis models

In order to design appropriate cell topologies and dimensions for thermal and structural performance requirements, it is necessary to establish techniques for evaluating the properties of prismatic cellular materials. Finite difference and finite element analysis – two approaches for quickly evaluating thermal performance in terms of total rates of steady-state heat transfer – are reviewed briefly in Section 3.1, followed by methods for determining overall structural elastic stiffness and critical buckling load in Section 3.2.

3.1. CONVECTIVE HEAT TRANSFER ANALYSIS

We present two approaches for analyzing convective heat transfer in the laminar regime within the prismatic cellular material. The first is a three-dimensional finite difference approach and the second is a two-dimensional finite element approach. Both of the approaches are more approximate but faster than FLUENT CFD analyses and therefore useful for rapid exploration of the design space for the present application. The finite element approach is less accurate than the finite difference method, but it is also more computationally efficient and easily generalized for variable cell shapes or topologies.

3.1.1. Three-dimensional finite difference heat transfer analysis

The finite difference method is a numerical technique for solving the three-dimensional steady state heat transfer equations – Fourier's law (conduction), Newton's law of cooling (convection), and an energy balance for the internal flow – associated with the sample prismatic cellular heat exchanger shown in Figure 1 [7]. Laminar flow is assumed. Complete details of the formulation and validation are provided by Dempsey and coauthors [8, 9]. The prismatic cellular material is discretized spatially using a set of nodal points located distances Δx and Δy apart in a cross section in the x - y plane, as shown in Figure 3. Cross-sections are repeated at regular intervals, Δl , along the length of the prismatic cellular material in the z -direction in Figure 1. A uniform temperature is designated for the fluid in each incremental length, Δl , of a cell and for each cell wall segment between nodes. Nodal spacing is dictated by cell sizes as graded cell dimensions may vary within a cross-section. By evaluating the energy balance for each node and utilizing central difference approximations with second order accuracy, a linear system of algebraic equations is constructed and then solved to obtain the temperature at each node. The exit temperature, T_{exit} , of the

fluid in each cell, i , can be used to calculate the total rate of steady state heat transfer, \dot{Q}_{total} , by a summation over all of the cells

$$\dot{Q}_{\text{total}} = \sum_i^{n_{\text{cells}}} \dot{m}_{\text{cell}_i} c_p (T_{\text{exit}_i} - T_{\text{in}}), \quad (1)$$

where \dot{m}_{cell_i} , T_{in} , and c_p are the mass flow rate in cell i , inlet fluid temperature, and specific heat of the fluid, respectively. The finite difference heat transfer analysis has been validated with physical experiments, analytical solutions, and FLUENT CFD simulations for both uniform and dimensionally graded cellular configurations [8, 9].

3.1.2. Two-dimensional finite element heat transfer analysis

A two-dimensional finite element approach is developed for modeling the three-dimensional convective heat transfer problem in an approximate but rapid manner. Complete details of the approach are provided by Kumar and McDowell [10]. The approach is based on a homogenization method. As illustrated in Figure 4, a two-dimensional cross-section of a prismatic cellular material at its inlet is discretized into a number of homogeneous, 4-node, linear finite elements. The void and associated fluid flow through each element are modeled implicitly via a distributed sink in the element. The governing finite element equation for an element domain Ω^e with flux boundary $\partial\Omega_h^e$ is given by:

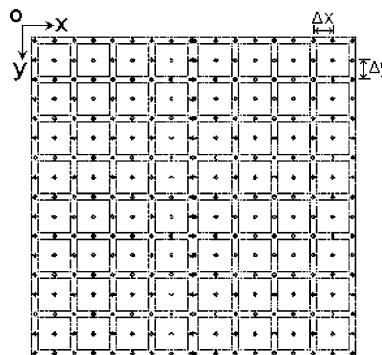


Figure 3. FD nodal placement on a typical cross-section of cellular material.

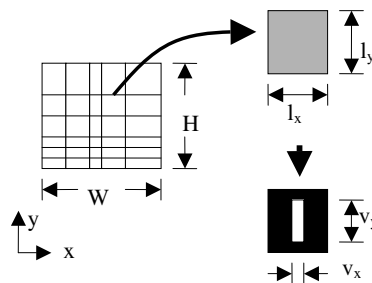


Figure 4. Two-dimensional homogenized FE approach. Discretization of a cellular material cross-section into homogeneous, 4-node, linear finite elements.

$$\begin{aligned} & \left(\int_{\Omega^e} [B^e]^T [D^e] [B^e] L_z dA + \int_{\Omega^e} \alpha_{\text{eff}}^e [N^e]^T [R^e] dA \right) \{T^e\} \\ & = - \int_{\Omega_h^e} [N^e]^T h^e L_z ds + \int_{\Omega^e} \alpha_{\text{eff}}^e [N^e]^T T_{\text{in}} dA, \end{aligned} \quad (2)$$

where $[N^e]$, $[B^e]$ and $[D^e]$ are element shape function, gradient of shape function and effective conductivity matrices, respectively, and the element nodal temperature is represented by vector $\{T^e\}$. The fluid inlet temperature is T_{in} , the applied normal heat flux is given by h^e and L_z is the out-of-plane dimension of the LCA. The average void temperature at the inlet is interpolated from the element nodal temperature using the matrix $[R^e]$. In this equation, the second term on both sides is due to the effect of out-of-plane heat convection through the voids. The sink strength, α_{eff}^e , in each element is calculated by solving a three-dimensional micromechanics problem of heat transfer through a rectangular duct. The walls of the duct are assumed to be isothermal so that an analytical solution can be utilized for the sink strength, i.e.

$$\alpha_{\text{eff}}^e = \frac{\dot{m}_{\text{cell}}^e c_p}{A^e} \left(1 - e^{-(\alpha^e P^e D)/(\dot{m}_{\text{cell}}^e c_p)} \right), \quad (3)$$

where \dot{m}_{cell}^e is the mass flow rate through the void associated with the element, A^e is the element planar area, D is the length of the duct, and P^e is the flow perimeter of the void. The laminar flow convection coefficient, α^e , can be obtained for a given fluid and void size and shape [7].

The assumption of isothermal walls in each cell leads to an upper-bound solution to the total heat transfer rate. The algorithm is implemented in MATLAB [11] and has been validated by comparison with three-dimensional finite difference solutions for a range of uniform and graded rectangular cell configurations. The equivalent homogenized modeling of the convection through the cells as heat sinks in the two-dimensional cross-section reduces computational time and can be extended to a more general continuum field approach.¹

3.2. STRUCTURAL ANALYSIS

Several authors have reported in-plane elastic properties and initial buckling loads for two-dimensional cellular materials with periodic hexagonal, square, rectangular, or triangular topologies [1, 2, 5, 12]. These analytical estimates are not appropriate, however, for the *non*-periodic cellular topologies explored in this example. Here, we outline approaches for assessing the overall structural elastic stiffness and critical buckling loads of such non-periodic, rectangular, prismatic, cellular materials.

3.2.1. Elastic stiffness estimates

When a prismatic cellular material with non-periodic rectangular cells is loaded along one of the coordinate axes in Figure 3, elastic deformation occurs due to axial

¹A more general continuum field approach would involve associating a number of cells with each element. Such an approach would be suitable for problems where the domain size is much larger than the cell size so that the behavior of a material point (integration point in a finite element model) is governed by variables characterizing the cell topology associated with that material point. However, in the present case each element is associated with only one rectangular void, rendering the post-processing step trivial.

extension or compression of the cell walls. If the loading is axial, and there are no imperfections in the structure, there is no bending contribution to the deformation in this particular loading configuration. Thus, the overall structural elastic stiffness in the x -direction (\tilde{E}_x) or y -direction (\tilde{E}_y) is approximated as the fraction of the total structural width (W) or height (H), respectively, occupied by cell walls, i.e.,

$$\tilde{E}_x/E_s \cong \frac{t_H(N_v + 1)}{H}, \quad (4)$$

$$\tilde{E}_y/E_s \cong \frac{t_v(N_H + 1)}{W}, \quad (5)$$

where E_s is the elastic modulus of the isotropic solid cell wall material.

3.2.2. Elastic buckling analysis

The cell walls of rectangular, prismatic, cellular materials can be quite slender. Furthermore the manufacturing process usually leads to a certain amount of imperfections in the cell walls. Both of these may result in elastic buckling failure under applied loading conditions. As the cellular material is subjected to a uniformly distributed load applied on the top surface with the bottom surface fixed, we consider two-dimensional analysis in the x - y plane. The critical buckling load is obtained by performing an eigenvalue buckling analysis in ABAQUS finite element program [13] with the cell walls modeled using Euler–Bernoulli beam elements. The first eigenvalue obtained from the analysis corresponds to the critical buckling load (assumed to be uniformly distributed on the top surface) of the material shown in Figure 1.

4. Multiobjective design approach

Since we are concerned with designing prismatic cellular materials that satisfy specified performance requirements and span multi-physics problem domains – in this case, heat transfer and elastic stiffness and buckling – a multifunctional, multiobjective design approach is required. In a multifunctional design process, as outlined in Figure 5, we begin with a set of overall design requirements and end with a set of multifunctional design specifications. To produce this transformation, we formulate and solve a compromise Decision Support Problem (DSP) – a hybrid multiobjective construct that incorporates concepts from both traditional mathematical programming and goal programming [14]. The compromise DSP is used to determine the values of design variables that satisfy a set of constraints and bounds and achieve a set of conflicting, multifunctional goals as closely as possible. It is solved using solution algorithms that are paired with appropriate domain-specific analysis models. In this paper, we are interested in two examples: (1) designing prismatic cellular materials that meet requirements for heat transfer rate and elastic stiffness, and (2) designing prismatic cellular materials that meet requirements for heat transfer rate and critical elastic buckling load. The analysis codes used in the different domains of analysis are very different. For the first example, user-developed Fortran and Basic computer programs are used while commercially available MATLAB and ABAQUS software are used for the second example. In order to perform multiobjective design, disparate software entities are integrated with commercial design/analysis integration software.

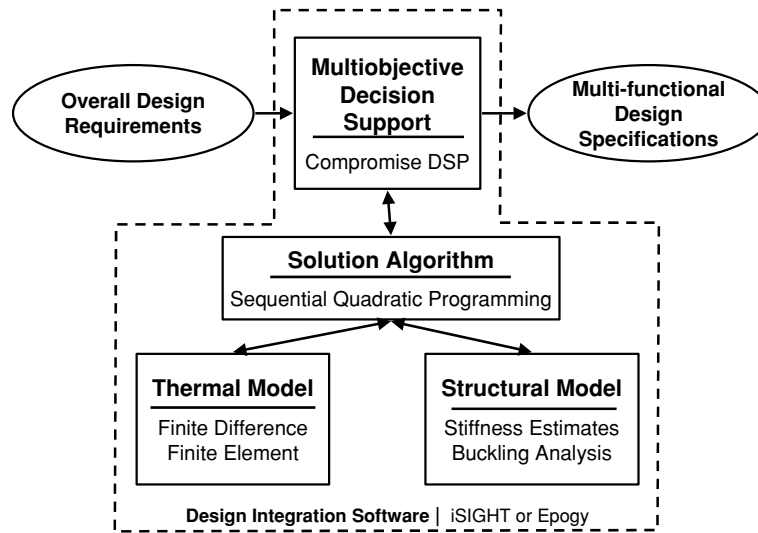


Figure 5. Multifunctional design approach.

To implement the design approach for this example, we begin by formulating the compromise DSP, as shown in Figure 6. As formulated in Figure 6, the objective is to determine the values of a set of design variables that satisfy a set of constraints and achieve a set of potentially conflicting goals as closely as possible for a specified set of boundary conditions and dimensions (Table 1). The design variables include the numbers of cells in the horizontal and vertical directions, N_H and N_V , the thickness of horizontal and vertical cell walls, t_H and t_V , the internal height of each row of cells, h_i , and the total mass flow rate, \dot{M} . Each column of cells is assumed to have identical internal width, w , which is a dependent variable that is a function of the total width, W , of the device and the variable thickness of the vertical cell walls, t_V , according to Eq. (7) in Figure 6. Compatibility constraints on the design include restrictions (Eqs. (7) and (8) in Figure 6) that ensure that the cells and cell walls fit together and occupy the overall dimensions of the device. Pressure drop and mass flowrate are related according to the fan curve of Figure 2, expressed as Eq. (6), and laminar flow is enforced in each cellular passageway. Together, the design variables and the set of inviolable constraints and bounds define the design space of feasible, potential solutions. Within the feasible design space, preferred solutions achieve

Table 1. Boundary conditions and dimensions for design

Structure Width (W)	0.025 m
Structure Height (H)	0.025 m
Structure Depth (D)	0.075 m
Inlet Air Temperature (T_{in})	293.15 K
Heat Source Temperature (T_s)	373.15 K
Conductivity of Solid Material (k)	363 W/m-K
Total Mass Flowrate (\dot{M})	Variable, Tied to Δp via Fan Curve (Figure 2)
Working Fluid	Air

Given

 Thermal and Structural Analysis Algorithms (Section 3)
 Boundary Conditions (Table 1)

Find
 $N_H, N_V, t_H, t_V, \dot{M}, h_1, h_2, \dots, h_{N_V}$
Satisfy
Constraints:

 Fan Curve (Figure 2): $\Delta P \leq 30 - (2663.35 * \dot{M})$ Eqn. 6
 $Re \leq 2300$

$$wN_H + t_V(N_H + 1) = W \quad \text{Eqn. 7}$$

$$\sum_{i=1}^{N_V} h_i + t_H(N_V + 1) = H \quad \text{Eqn. 8}$$

System Goals:

$$\frac{\dot{Q}_{total}}{\dot{Q}_{total-target}} + d_1^- - d_1^+ = 1 \quad \text{Eqn. 9}$$

$$\frac{\tilde{E}_y / E_s}{(\tilde{E}_y / E_s)_{target}} + d_3^- - d_3^+ = 1 \quad \text{Eqn. 11}$$

$$\frac{\tilde{E}_x / E_s}{(\tilde{E}_x / E_s)_{target}} + d_2^- - d_2^+ = 1 \quad \text{Eqn. 10}$$

$$\frac{f_y}{f_{y-target}} + d_4^- - d_4^+ = 1 \quad \text{Eqn. 12}$$

Bounds on Design Variables:

Common	Heat transfer & Elastic stiffness	Heat transfer & Elastic buckling
$2 \leq N_H \leq 16$	$0.00025 \text{ m} \leq h_i \leq 0.022 \text{ m}$	$0.002 \text{ m} \leq h_i \leq 0.022 \text{ m}$
$2 \leq N_V \leq 16$	$0.00015 \text{ m} \leq t_H \leq 0.002 \text{ m}$	$0.00015 \text{ m} \leq t_H \leq 0.0005 \text{ m}$
$d_i^+, d_i^- \geq 0$	$0.00015 \text{ m} \leq t_V \leq 0.002 \text{ m}$	$0.00015 \text{ m} \leq t_V \leq 0.0005 \text{ m}$
$d_i^+ \cdot d_i^- = 0$	$0.0005 \text{ kg/s} \leq \dot{M} \leq 0.003 \text{ kg/s}$	$0 \text{ kg/s} \leq \dot{M} \leq 0.0113 \text{ kg/s}$

Minimize

$$Z = W_1 d_1^- + W_2 d_2^- + W_3 d_3^- + W_4 d_4^- \quad \text{Eqn. 13}$$

(See Tables 2 and 3 for weights and target values.)

Figure 6. Compromise DSP formulated for structural heat exchanger design.

a set of potentially conflicting, multifunctional goals as closely as possible. For this design, there are four goals, all of which are maximized: total rate of steady state heat transfer, \dot{Q}_{total} (Eqs. (1) and (9)), overall structural elastic stiffness in the horizontal and vertical directions, \tilde{E}_x/E_s and \tilde{E}_y/E_s , expressed as fractions of the elastic modulus of the solid cell wall material, E_s (Eqs. (4), (5), (10) and (11)), and critical buckling load, f_y (Eq. (12)). Deviation variables d_i^- and d_i^+ measure the extent to which each goal, i , achieves an ambitious target value (e.g. $\dot{Q}_{total-target}$ in Figure 6) in Eqs. (9)–(12). The deviation variables for all goals are combined into an objective function, which measures the extent to which multiple goals are achieved. This approach differs from classical single-objective optimization with imposed constraints. In Figure 6, the objective function is expressed in Eq. (13) as a weighted sum of relevant deviation variables, although other formulations are possible [14]. The weights and target values for each goal are recorded along with the results in Section 5. After the problem is formulated, it must be solved using appropriate domain-specific analyses and software codes coupled with solution or search algorithms, as illustrated in Figure 5.

5. Results and discussion

The compromise DSP is solved for two distinct design scenarios. In the first design scenario (with results reported in Table 2), finite difference heat transfer analysis and elastic structural stiffness analysis are used to evaluate the performance of the structural heat exchanger as described in Sections 3.1 and 3.2. The compromise DSP is solved using a sequential quadratic programming solution algorithm for searching the design space. iSIGHT design integration software [15] interfaces domain-specific analysis software – customized codes written in Fortran and Visual Basic – with solution algorithms guided by the mathematical formulation of the compromise DSP illustrated in Figure 6. In the second design scenario (with results reported in Table 3), the goals are the total rate of steady state heat transfer and the critical buckling load for the material. A MATLAB code is used to perform finite element heat transfer analysis and eigenvalue buckling analysis is conducted using ABAQUS, as described in Sections 3.1 and 3.2. The compromise DSP is solved using Epogy software [16] that integrates heterogeneous analysis codes in addition to performing search. Epogy uses a hybrid optimizer consisting of a combination of genetic, downhill simplex, gradient and linear simplex algorithms.

Design results are recorded in Tables 2 and 3 for the first and second design scenarios, respectively. The total heat transfer rates for the two design scenarios differ due to the distinct analysis models – three-dimensional finite difference and two-dimensional finite element analysis – adopted for the studies in Tables 2 and 3, respectively. As discussed earlier, the two-dimensional finite element model leads to an upper bound estimate of the total heat transfer rate [10]. Thus, the total rates of steady state heat transfer reported in Table 3 are slightly higher than those reported in Table 2 for very similar cellular mesostructures. The total rates of steady state heat transfer predicted by the finite difference simulation in Table 2 are more accurate when compared with experimental and computational fluid dynamics results. Although the magnitudes of the heat transfer rate estimates differ for the two analysis approaches, the nature of the resulting designs is very similar as can be seen by comparing uniform or graded designs for 14×2 or 14×3 cellular mesostructures in Table 2 with equivalent results reported in Table 3. This justifies the use of computationally efficient approximate models for rapid preliminary designs. Once an optimal design is identified using the two-dimensional approach, the total heat transfer rate can be evaluated and verified via more accurate schemes such as three-dimensional finite difference or computational fluid dynamics. Another strategy is to use the two-dimensional model to rapidly identify regions of the design space that are near-optimal, and then exercise more computationally intensive three-dimensional codes to conduct the final search procedures (i.e., detail design).

Results in the first and second columns of each table are obtained by maximizing only the total rate of steady state heat transfer (i.e., the first goal in Figure 6) for uniform and graded cell dimensions, respectively. Since the numbers of cell rows and columns are discrete variables that are not accommodated easily by gradient-based solution algorithms, the design process is repeated for alternative discrete numbers of rows and columns. The designs with the largest heat transfer rates – 14×2 and 14×3 configurations – are reported in Tables 2 and 3 and refined (with fixed numbers of rows and columns) for multifunctional trade-offs between the total rate of

Table 2 – Example Results for Case 1 (Effective Elastic Stiffness and Heat Transfer with 3D Finite Difference Analysis)

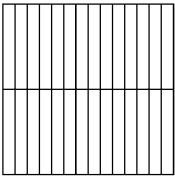
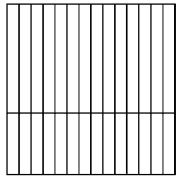
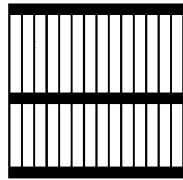
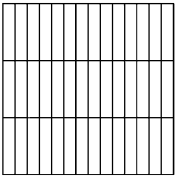
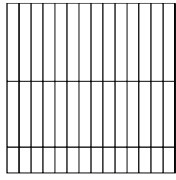
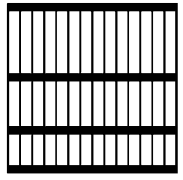
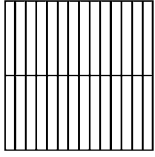
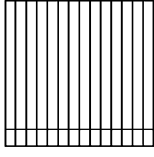
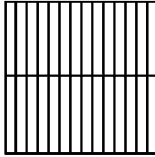
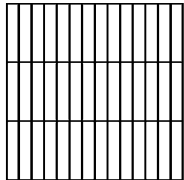
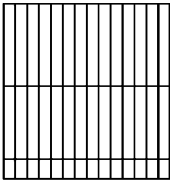
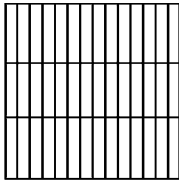
14 columns x 2 rows--Heat Transfer and Elastic Stiffness		
Uniform cell heights	Graded cell heights	Multiobjective design
		
<p>Weights and Targets: $\mathbf{W} = \{1.0, 0, 0, 0\}$ $\dot{Q}_{total-target} \gg \dot{Q}_{total}$</p> <p>Design Variable Values: $h = 12.26$ mm $w = 1.59$ mm $t_V = 0.18$ mm $t_H = 0.16$ mm</p> <p>Goal Values: $\tilde{E}_x / E_s = 0.02$ $\tilde{E}_y / E_s = 0.11$ $\dot{Q}_{total} = 112.99$ W</p>	<p>Weights and Targets: $\mathbf{W} = \{1.0, 0, 0, 0\}$ $\dot{Q}_{total-target} \gg \dot{Q}_{total}$</p> <p>Design Variable Values: $h = 15.73, 8.79$ mm $w = 1.59$ mm $t_V = 0.18$ mm $t_H = 0.16$ mm</p> <p>Goal Values: $\tilde{E}_x / E_s = 0.02$ $\tilde{E}_y / E_s = 0.11$ $\dot{Q}_{total} = 113.13$ W</p>	<p>Weights and Targets: $\mathbf{W} = \{0.5, 0.25, 0.25, 0\}$ $\dot{Q}_{total-target} = 110$ W $(\tilde{E} / E_s)_{target} = 0.20$</p> <p>Design Variable Values: $h = 11.10, 9.01$ mm $w = 1.48$ mm $t_V = 0.28$ mm $t_H = 1.63$ mm</p> <p>Goal Values: $\tilde{E}_x / E_s = 0.17$ $\tilde{E}_y / E_s = 0.20$ $\dot{Q}_{total} = 91.62$ W</p>
14 columns x 3 rows—Heat Transfer and Elastic Stiffness		
Uniform cell heights	Graded cell heights	Multiobjective design
		
<p>Weights and Targets: $\mathbf{W} = \{1.0, 0, 0, 0\}$ $\dot{Q}_{total-target} \gg \dot{Q}_{total}$</p> <p>Design Variable Values: $h = 8.13$ mm $w = 1.60$ mm $t_V = 0.17$ mm $t_H = 0.15$ mm</p> <p>Goal Values: $\tilde{E}_x / E_s = 0.02$ $\tilde{E}_y / E_s = 0.11$ $\dot{Q}_{total} = 109.15$ W</p>	<p>Weights and Targets: $\mathbf{W} = \{1.0, 0, 0, 0\}$ $\dot{Q}_{total-target} \gg \dot{Q}_{total}$</p> <p>Design Variable Values: $h = 11.30, 9.50, 3.64$ mm $w = 1.60$ mm $t_V = 0.17$ mm $t_H = 0.15$ mm</p> <p>Goal Values: $\tilde{E}_x / E_s = 0.02$ $\tilde{E}_y / E_s = 0.11$ $\dot{Q}_{total} = 109.91$ W</p>	<p>Weights and Targets: $\mathbf{W} = \{0.5, 0.25, 0.25, 0\}$ $\dot{Q}_{total-target} = 110$ W $(\tilde{E} / E_s)_{target} = 0.20$</p> <p>Design Variable Values: $h = 9.10, 6.55, 4.51$ mm $w = 1.48$ mm $t_V = 0.28$ mm $t_H = 1.21$ mm</p> <p>Goal Values: $\tilde{E}_x / E_s = 0.17$ $\tilde{E}_y / E_s = 0.19$ $\dot{Q}_{total} = 88.47$ W</p>

Table 3 – Example Results for Case 2 (Critical Buckling Load and Heat Transfer with 2D Finite Element Analysis)		
14 columns x 2 rows—Heat Transfer and Critical Buckling Load		
<p>Uniform cell heights</p> 	<p>Graded cell heights</p> 	<p>Multiobjective design</p> 
<p>Weights and Targets: $\mathbf{W} = \{1.0, 0, 0, 0\}$ $\dot{Q}_{total-target} \gg \dot{Q}_{total}$</p> <p>Design Variable Values: $h = 12.27$ mm $w = 1.56$ mm $t_V = 0.22$ mm $t_H = 0.15$ mm</p> <p>Goal Values: $f_y = 3.19$ MPa $\dot{Q}_{total} = 114.7$ W</p>	<p>Weights and Targets: $\mathbf{W} = \{1.0, 0, 0, 0\}$ $\dot{Q}_{total-target} \gg \dot{Q}_{total}$</p> <p>Design Variable Values: $h = 21.85, 2.7$ mm $w = 1.57$ mm $t_V = 0.20$ mm $t_H = 0.15$ mm</p> <p>Goal Values: $f_y = 0.87$ MPa $\dot{Q}_{total} = 115$ W</p>	<p>Weights and Targets: $\mathbf{W} = \{0.5, 0, 0, 0.5\}$ $\dot{Q}_{total-target} = 140$ W $(f_y)_{target} = 10.00$ MPa</p> <p>Design Variable Values: $h = 11.80, 12.40$ mm $w = 1.45$ mm $t_V = 0.31$ mm $t_H = 0.25$ mm</p> <p>Goal Values: $f_y = 10.1$ MPa $\dot{Q}_{total} = 109.7$ W</p>
14 columns x 3 rows—Heat Transfer and Critical Buckling Load		
<p>Uniform cell heights</p> 	<p>Graded cell heights</p> 	<p>Multiobjective design</p> 
<p>Weights and Targets: $\mathbf{W} = \{1.0, 0, 0, 0\}$ $\dot{Q}_{total-target} \gg \dot{Q}_{total}$</p> <p>Design Variable Values: $h = 8.13$ mm $w = 1.55$ mm $t_V = 0.22$ mm $t_H = 0.15$ mm</p> <p>Goal Values: $f_y = 6.16$ MPa $\dot{Q}_{total} = 111.7$ W</p>	<p>Weights and Targets: $\mathbf{W} = \{1.0, 0, 0, 0\}$ $\dot{Q}_{total-target} \gg \dot{Q}_{total}$</p> <p>Design Variable Values: $h = 11.56, 10.20, 2.65$ mm $w = 1.55$ mm $t_V = 0.22$ mm $t_H = 0.15$ mm</p> <p>Goal Values: $f_y = 3.58$ MPa $\dot{Q}_{total} = 112.4$ W</p>	<p>Weights and Targets: $\mathbf{W} = \{0.5, 0, 0, 0.5\}$ $\dot{Q}_{total-target} = 140$ W $(f_y)_{target} = 10.00$ MPa</p> <p>Design Variable Values: $h = 8.30, 7.48, 8.58$ mm $w = 1.51$ mm $t_V = 0.26$ mm $t_H = 0.17$ mm</p> <p>Goal Values: $f_y = 10.1$ MPa $\dot{Q}_{total} = 110.8$ W</p>

steady state heat transfer and either overall elastic structural stiffness or critical buckling load, as reported in the third column of Tables 2 and 3, respectively.

As shown in the tables, graded designs achieve slightly higher overall rates of steady state heat transfer than uniform designs. Cells near the top of the device – where the heat source is located – tend to elongate to facilitate heat transfer. For the first and second columns of results – for which only heat transfer is maximized – cell walls tend to be very thin, resulting in high overall rates of steady state heat transfer but low overall structural elastic stiffness and critical buckling loads. It is apparent in Tables 2 and 3 that the multifunctional designs in the third column have thicker walls in order to achieve higher overall elastic structural stiffness or critical buckling loads. For the design involving heat transfer and effective elastic structural stiffness in Table 2, the horizontal cell walls are considerably thicker in order to achieve balanced elastic stiffness properties in x - and y - directions. In the design scenario involving heat transfer and elastic buckling in Table 3, the cell walls are again thicker. In addition, the vertical dimensions of the cells near the heat source (also the edge on which the uniformly distributed load is applied) tend to be less elongated in order to achieve the target elastic buckling load. An interesting aspect of the results in Table 3 is that the 14×3 multifunctional mesostructure has greater heat transfer rates than the 14×2 multifunctional mesostructure for the same buckling load. By using more cells in the y -direction, it can achieve the same buckling load with thinner vertical cell walls that offer enhanced heat transfer characteristics.

There is a tradeoff between structural and thermal properties for both design scenarios. With smaller cell sizes, larger cell wall thicknesses, and more uniform cell dimensions in the multifunctional designs, a portion of the total heat transfer rate is sacrificed to achieve higher stiffness or buckling load. By adjusting weights and target values in the objective function of Eq. (13), it is possible to generate a family or Pareto set of designs with a range of tradeoff values between the multiple objectives for a specific set of boundary conditions. The weights and target values for this example are recorded in Tables 2 and 3, with the vector of weights corresponding to the objective function of Eq. (13).

6. Extension to broad classes of materials design problems

The foregoing framework of multiobjective decision support for designing materials can be readily extended to incorporate the design of the material (composition, morphology, etc.) as part of a larger overall systems design process. By employing substructuring (variable resolution analyses) or homogenization concepts, material behavior at multiple length scales and time scales can be analyzed as necessary to provide decision support for selection of hierarchical morphology and process path to deliver a required set of multifunctional, often conflicting properties. It is our view that too often major materials development programs are set forth which aim to achieve one or two primary properties or requirements (e.g. high temperature strength or creep resistance of alloys), defined in isolation from the overall systems context (e.g. corrosive/oxidative operating environment) or any notion of how strongly these properties may be coupled with other secondary, but still critical, properties (e.g. thermo-mechanical or low cycle fatigue resistance).

Moreover, the same framework can embody the hierarchy of process-structure-properties-performance set forth by Olson [17], shown in Figure 7. The inductive goals/means engineering approach is relevant to design, and contrasts with the usual approach taken in application of the scientific method, which focuses on deductive cause-and-effect (bottom-up). While Olson's construct sets an important philosophical foundation on which to support materials science and materials design, it delegates the practical aspects of process-structure, structure-property and property-performance assessment to the creative will, depth of insight, experience and knowledge base of the designer. To render the philosophy robust and collaborative, it must be built upon a systems-engineering framework. Without such a framework in which to embed performance-properties-structure-processing relations, manage information flow, interrogate models, explore variability, and engage decision-support protocols to facilitate choice among alternatives, materials design may be more of an art than a science.

We can map Olson's inductive goals/means concept of materials design directly to the systems-based approach adopted in the present work, as indicated in Figure 8. It can be extended directly to the design of more complex, multifunctional, multiscale material systems as illustrated in Figure 9. As shown in the figures, process-structure-property relations inform the designer and map directly into the design process that facilitates transformation of overall design requirements into a set of robust specifications for the material system of interest.

As shown in Figure 8, a design process generally begins with specification of the overall performance requirements for the design and formulation of a design space of potential solutions. As input for the present design process, we have requirements such as total heat transfer, stiffness, and buckling resistance subject to constraints on maximum weight, cost etc. To define the design space for this application, process-structure relations were invoked implicitly by selecting copper (based on oxide powders that can be reduced in the extrusion process to yield near fully dense metal with high thermal conductivity and acceptable strength) and imposing additional constraints on minimum wall thicknesses and aspect ratios (thickness to length ratios) that lead to extrusions with high probability of achieving target mechanical integrity in the reduced and sintered honeycomb form. Process-structure relations, derived both from experiential process maps and from computational tools rooted in thermodynamics and kinetics, inform the design process by establishing whether feasible

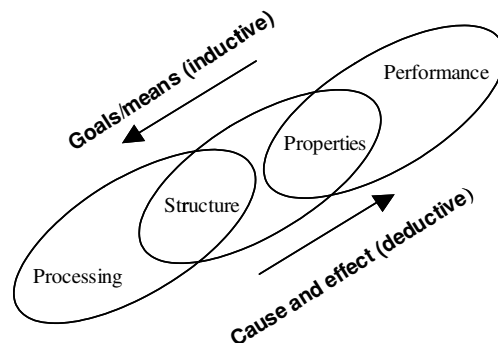


Figure 7. Olson's hierarchical concept of 'Materials by Design' [17].

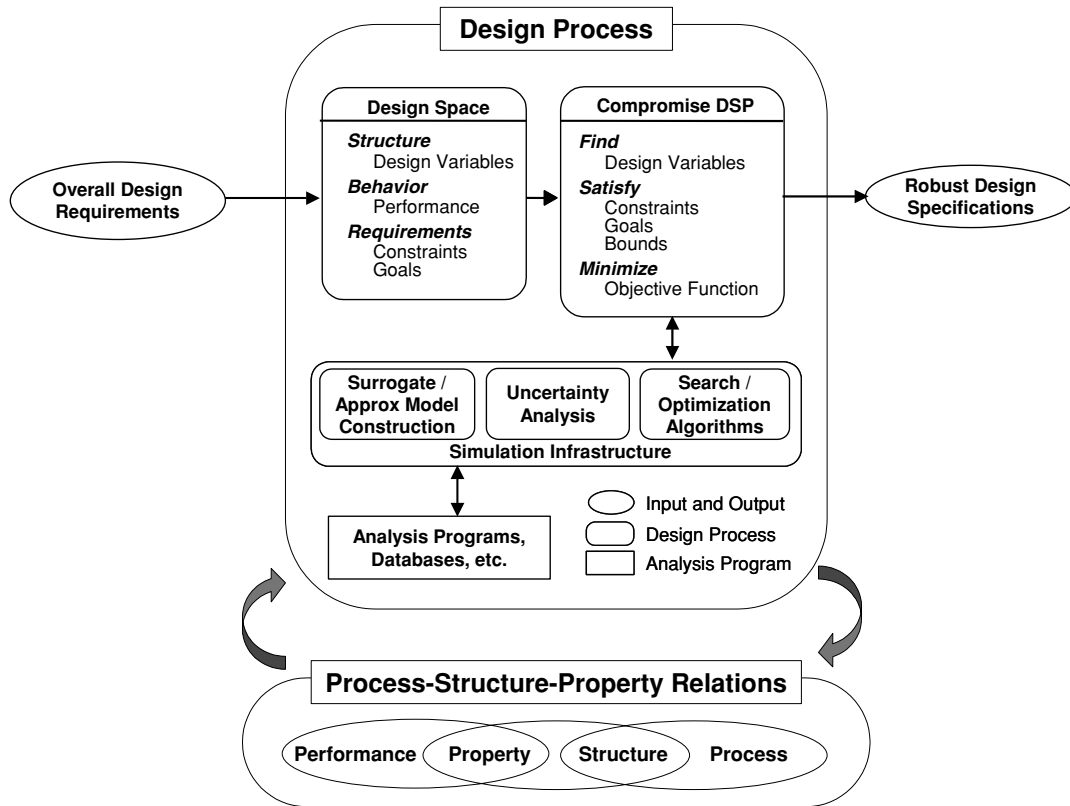


Figure 8. A systems-based materials design approach.

process paths exist for the compositions and morphologies of interest and serve to demarcate the subset of the overall design space which may be associated with *feasible solutions*. Since it is reasonable to explore only the space of feasible solutions, and since the families of solutions in multiobjective design that satisfy design requirements typically lie on or close to the boundaries of the feasible subset of the entire design space, it is important to identify at the outset of the design process (i) whether such regions exist, and (ii) the extent of their domain. These regions then serve to constrain exploration of the design space via computational structure-property tools to much more limited domains near the boundaries of feasible microstructures – a practical necessity due to the intensive nature of many of the structure-property codes. The *design space* is a multidimensional hyperspace with design variables as coordinates, the feasible subset of which is bounded by a faceted hypersurface or by families of simply-connected but distinct hypersurfaces. Due to the non-linearity and complexity of the resulting design space, it cannot be categorically stated that multiobjective designs will be located at vertices or intersections of multi-faceted hypersurfaces; other criteria, such as robustness of solutions, may be applied to identify acceptable Pareto solutions. Hence, exploration must be performed over the entire vicinity of the feasible subspace boundaries.

As shown in Figure 8, design exploration is facilitated by formulating and solving a compromise DSP, which mathematically models the multiobjective decision associated with the feasible design space. It is solved using a combination of simulation

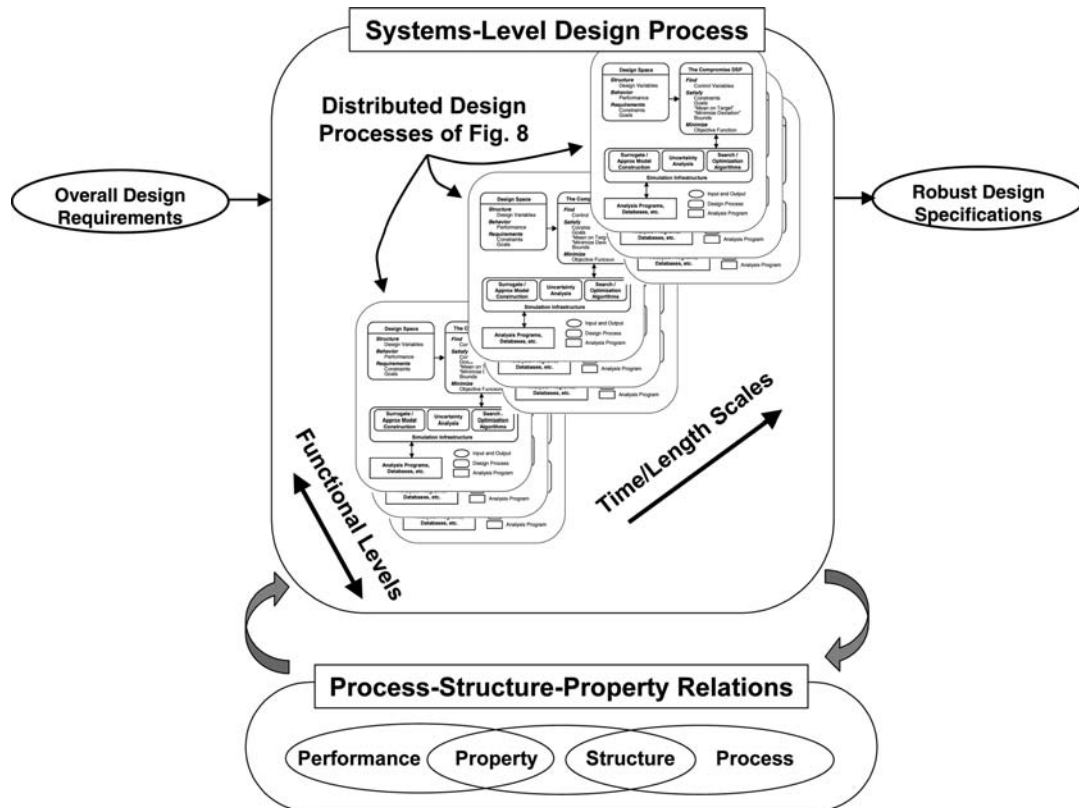


Figure 9. Systems-based approach for design of multiscale, multifunctional materials.

infrastructure (solution algorithms, surrogate or approximate models used in place of complex analysis models for efficient design space exploration, statistical analysis of variability, etc.) and analysis programs, models, and databases. In our example, we used commercial design integration software for integrating the compromise DSP with solution algorithms and analytical models. The computational or analytical models were used to determine structure-property relations (e.g. effective structural elastic stiffness, conductivity and convective heat transfer). In general, the functions of these analytical models/codes within our systems-based approach can be classified according to Olson's hierarchy in Figure 7:

- *Process-structure relations*: Establish manufacturing constraints (processes, available process equipment, etc.), cost factors, thermodynamic feasibility (favorable, unfavorable microstructures; stable, metastable, unstable), kinetic feasibility (feasibility of rates of process, necessary driving forces, and long term stability of metastable microstructures).
- *Structure-property relations*: Relate composition, phase and morphology information, expressed using distribution functions or digital representations amenable to computation, to response functions that relate to properties of relevance to the design. This is most often intrinsically an hierarchical modeling exercise.
- *Property-performance relations*: Relate feasible properties to response functions that are relevant to imposed performance requirements, either through detailed point-by-point computational models or by construction of approximate

response surface or surrogate models, depending on the degree of computational intensiveness.

It is apparent that the philosophy outlined in Figure 7 and its relation to our systems-based design approach resonates with the modern foundation of materials science, built on the triad of process-structure-properties, adding performance requirements to form the linkage to applications.

While the design process in Figure 8 is depicted as a simplified process for a single design stage and a single decision-maker, it may be necessary to formulate and solve a hierarchy of compromise DSPs for complex material systems using analysis models associated with a hierarchy of length and time scales and multiple functional domains. This is illustrated in Figure 9 in which each of the layered boxes represents a separate instantiation of the design process depicted in Figure 8. Clearly, a design process applied at any *one* level of the hierarchical design process cannot, in general, produce robust designs that meet requirements for the entire system. A systems-based framework is required in which to integrate process-structure-property-performance relations, information flow, distributed computing resources, and decision-based protocols throughout the hierarchical design space shown in Figure 9. We are currently developing the intellectual and computing infrastructure to address many of these challenges, but those topics are addressed elsewhere (cf. [18–21]).

7. Closure

A systems-based multiobjective approach has been presented for designing non-uniform, graded cellular material mesostructure for superior multifunctional performance. The design approach is based on multiobjective decision models that are integrated with search/solution algorithms and multi-physics analysis models of structural and heat transfer performance. The compromise DSP facilitates structuring the design problem. By solving a decision support problem, material mesostructures – including graded dimensions and aspect ratios of cells and cell walls – are synthesized that satisfy a set of constraints and achieve as closely as possible a set of potentially conflicting, multifunctional goals. The compromise DSP is solved using search/solution algorithms that query multi-physics models to evaluate the multifunctional performance of alternative designs. Approximate analysis models – in this case including three-dimensional finite difference and two-dimensional finite element models – are presented and utilized for quickly evaluating heat transfer and elastic stiffness performance. While approximate models are less accurate than the detailed approaches embedded in many commercially available models, they facilitate multifunctional design by enabling computationally efficient evaluation of designs and therefore broader exploration of a complex design space. Commercially available software is used to integrate or coordinate use of disparate customized and commercial, multi-physics software resources.

The multifunctional design approach is used to design families or Pareto sets of non-uniform, graded prismatic cellular materials that embody a range of tradeoffs between conflicting thermal and structural performance objectives. The impact of considering multi-physics performance objectives is reflected in the cellular mesostructures and in their respective thermal and structural characteristics. When compared with materials

designed exclusively for thermal objectives, multifunctional designs have thicker walls and correspondingly improved structural properties (i.e., elastic stiffness and critical buckling loads), but thermal performance is sacrificed in terms of lower heat transfer rates for specified boundary conditions. By adjusting weights and or performance targets in the multiobjective decision model, it is possible to adjust the multifunctional tradeoff embodied in a cellular mesostructure.

Prismatic cellular materials are promising for a variety of innovative, high-impact, multifunctional applications – ranging from actively cooled structural elements for satellites or hypersonic aircraft wings to lightweight structural elements with internal damping characteristics achieved by polymer injection into selected cells. In future work, we anticipate extending and augmenting our multifunctional design approach to accommodate and synthesize a broader range of cellular topologies, variability in material structures and boundary conditions, and additional multi-physics analyses. We also plan to leverage our systems-based approach for designing complex material systems with a hierarchy of associated length and time scales to provide required multifunctional properties within a larger overall systems design process.

Acknowledgements

The authors acknowledge support from an AFOSR Multi-University Research Initiative (1606U81). C.C. Seepersad is sponsored by the Fannie and John Hertz Foundation. D.L. McDowell and R. Kumar gratefully acknowledge support of DARPA DSO (N00014-99-1-1016, L. Christodoulou) and ONR (N0014-99-1-0852, S. Fishman). F. Mistree and J. K. Allen gratefully acknowledge the support of the National Science Foundation through grant DMI-0085136.

References

1. Gibson, L.J. and Ashby, M.F., *Cellular Solids: Structure and Properties*, Cambridge University Press, Cambridge, UK, 1997.
2. Hayes, A.M., Wang, A., Dempsey, B.M. and McDowell, D.L., *Mech. Mater.*, 36(8) (2004) 691.
3. Evans, A.G., Hutchinson, J.W., Fleck, N.A., Ashby, M.F. and Wadley, H.N.G., *Prog. Mater. Sci.*, 46 (2001) 309.
4. Cochran, J.K., Lee, K.J., McDowell, D.L. and Sanders, T. H., In *Proceedings of the 4th Conference on Aerospace Materials, Processes, and Environmental Technology*, Huntsville, AL, (2000).
5. Gu, S., Lu, T.J. and Evans, A.G., *Int. J. Heat Mass Transfer*, 44 (2001) 2163.
6. Church, B.C., Dempsey, B.M., Clark, J.L., Sanders, T.H. and Cochran, J.K., In *Proceedings of IMECE 2001, International Mechanical Engineering Congress and Exposition*, New York, (2001).
7. Incropera, F.P. and DeWitt, D.P., *Fundamentals of Heat and Mass Transfer*, 3rd Edition, Wiley, New York, 1996.
8. Dempsey, B.M., M.S. Thesis, G.W. Woodruff School of Mechanical Engineering, Georgia Institute of Technology, Atlanta, GA, 2002.
9. Seepersad, C.C., Dempsey, B.M., Allen, J.K., Mistree, F. and McDowell, D.L. *AIAA J.*, 42 (2004) 1025.
10. Kumar, R.S. and McDowell, D.L., *AIAA J.*, 42 (2004) 1652.
11. MATLAB, Version 6.5, Release 13, The Math Works, Inc., Natick, MA, 2001.
12. Torquato, S., Gibiansky, L.V., Silva, M.J. and Gibson, L.J., *Int. J. Mech. Sci.*, 40 (1998) 71.
13. ABAQUS, Version 6.3-1, Abaqus, Inc., Pawtucket, RI, 2004.

14. Mistree, F., Hughes, O.F. and Bras, B.A., In Kamat, M.P. (Ed.) *Structural Optimization: Status and Promise*, AIAA, Washington, D.C., 1993, pp. 247–286.
15. iSIGHT, Version 7.0, Engineous Software, Inc., Cary, NC, 2003.
16. Epogy, Version 2003a, Synaps, Inc. (Part of Engineous Software, Inc.), Cary, NC, 2003.
17. Olson, G.B., *Science*, 277 (1997) 1237.
18. Choi, H.-J., Panchal, J.H., Rosen, D.W., Allen, J.K. and Mistree, F., In *Proceedings of the ASME Computers and Information in Engineering Conference*, Chicago, Illinois, (2003), Paper No. DETC2003/CIE-48279.
19. Fernandez, M.G., Rosen, D.W., Allen, J.K. and Mistree, F., In *Proceedings of the ASME Computers and Information in Engineering Conference*, Montreal, Canada, (2002), Paper No. DETC2002/CIE-34466.
20. Hernandez, G., Seepersad, C.C. and Mistree, F., *Eng. Optim.*, 34 (2002) 561.
21. Chen, W., Allen, J.K., Mavris, D. and Mistree, F., *Eng. Optim.*, 26 (1996) 137.